Submitted to J. of Chemical Physics

UCRL-19082
Preprint

DYNAMICS OF THE REACTION OF Ar^+ WITH D_2

M. Chiang, E. A. Gislason, B. H. Mahan,
C. W. Tsao, and A. S. Werner

September 1969

AEC Contract No. W-7405-eng-48

LAWRENCE RADIATION LABORATORY
UNIVERSITY of CALIFORNIA BERKELEY

UCRL-19082

DISCLAIMER

DYNAMICS OF THE REACTION OF Ar^+ WITH D_2.

M. Chiang, E. A. Gislason, B. H. Mahan,
C. W. Tsao, and A. S. Werner

Department of Chemistry and Inorganic Materials Research Division of the Lawrence Radiation Laboratory, University of California, Berkeley, California.

Abstract

We report measurements of the velocity vector distributions of the ionic products of collisions of Ar^+ with D_2 and He for relative energies between 2.26 and 9.1 eV. The ion ArD^+ is produced by a direct interaction mechanism which gives considerable forward scattering. The nonreactive scattering of Ar^+ by D_2 is intense, nearly elastic, and very similar to the scattering of Ar^+ by He. Differential reactive cross sections are determined, partially deconvoluted, and compared with results from several other laboratories.

As part of a series[1-5] of experimental investigations of the dynamics of gaseous ion-molecule reactions, we report here measurements of the energy and angular distribution of the ionic products of collisions of Ar^+ with D_2 and He. The reaction

$$Ar^+ + D_2 \rightarrow ArD^+ + D$$

has been studied many times with conventional mass spectrometers,[6,7] tandem mass spectrometers,[8] velocity analyzers,[9-12] and most recently with ion beam techniques[13,14] which permit both energy and angular analysis of the products. However, the present work is the first in which complete velocity vector distributions of reactively and nonreactively scattered ions have been determined.

EXPERIMENTAL

The instrument used in this work consists of a magnetic mass spectrometer for preparation of a collimated beam of primary ions of known energy, a scattering cell to contain the target gas, and an ion detection train made up of an electrostatic energy analyzer, a quadrupole mass filter, and an ion counter. The detector components and the exit slit of the scattering cell are mounted on a rotatable lid, which permits simultaneous angular and energy measurements on the ion products. These major components have been described in detail previously.[1,3,4] In all important respects, the constitution and operation of the apparatus, and the data

acquisition and reduction techniques were the same as we used in earlier work.

RESULTS

We performed twenty-five experiments in which either D_2 or He was the target gas. At relative energies of 2.75, 4.55, 6.83, and 9.13 eV, enough data were collected to permit construction of contour maps of the relative values of the specific intensity of Ar^+ and ArD^+ scattered from D_2, and Ar^+ scattered from He. Six of these twelve maps are shown in Figs. 1-6. The specific intensity $I_{cm}(\theta,u)$ is defined as the number of particles per second with a velocity in the center of mass system specified by u and θ, per unit beam intensity, scattering gas density, scattering length, and velocity space volume. As we[3] and others[15] have pointed out, this quantity is the same in the center of mass and laboratory coordinate systems. Of course, due to the finite resolution of the apparatus, the quantity plotted in Figs. 1-6 is actually $\bar{I}(\theta,u)$, the specific intensity averaged over the detector's volume in velocity space.

We can discern the general features of the reaction dynamics by examination of Figs. 1 and 4. The ArD^+ is distributed asymmetrically about the $\pm 90°$ line in the center of mass system and is strongly peaked at a center of mass system angle of zero, that is, in the direction of the original Ar^+ projectile. These features were found in earlier experiments by the groups

of Bailey[13] and Wolfgang.[14] The asymmetry about ±90° indicates that the reaction proceeds by a direct process in which the three atoms are simultaneously close to each other for less time than a period of rotation. The peaking of the intensity at very small angles suggests that, at least at these energies, the most probable reactive event is something akin to the ideal stripping process.[9] Indeed, as Figs. 1 and 4 show, for initial relative energies between 2.7 and 4.5 eV the product intensity maxima occur very close to the ideal stripping velocity

$$v = v_o M/(M+m),$$

where v_o is the laboratory projectile velocity, M is the projectile mass, and m is the mass of the abstracted atom. For lower initial relative energies, the groups of Bailey,[13] Wolfgang,[14] Fink,[12], and Henglein[11] have found product intensity maxima at velocities greater than the ideal stripping velocity. For relative energies greater than 5 eV, Bailey,[11] Henglein,[9] and ourselves (see Table I) find that the forward scattered product peaks at a velocity greater than the ideal stripping velocity. At the higher relative energies, the small reaction cross section and the limited resolution of the mass filter made detection of the small amount of mass 42 in a mass 40 background rather difficult. Consequently the location and shape of the forward peaks in the 6.83 and 9.13 eV experiments is less certain than at the lower energies.

Significant product intensity appears in Figs. 1 and 4 at center of mass angles greater than 90°. At the relative energies used in these experiments, products found at large scattering angles must be the result of small impact parameter collisions in which the incipient ArD^+ rebounds from the freed deuterium atom, and thereby acquires a velocity component opposite to the direction of approach of the Ar^+ projectile. We detected this large angle rebound scattering even at the lowest relative energy used (2.26 eV). Backscattering was evidently not detected at this energy in the ion-molecular beam experiments of Wolfgang.[14] In our apparatus, the use of a scattering cell with its attendant higher scattering gas density, and an electrostatic deflection ion-energy analyser with its superior discrimination properties, permit detection of the low intensity back scattered product even in the presence of a high intensity of forward scattered product.

The significance of the intensity distributions is made clearer by introduction of the translational exothermicity of the reaction Q, defined by

$$Q = \frac{1}{2}\mu' g'^2 - \frac{1}{2}\mu g^2$$

Here μ and g are, respectively, the reduced mass and relative speed of the reactants, and μ' and g' are the same quantities for the products. The assumption that the reactants are in their ground states allows us to write

$$Q = - \Delta E_o^o - U$$

$$Q(eV) = -2.3 + D\ (Ar\text{-}D^+) - U$$

where ΔE_o^o is the energy change for the reaction, U is the internal excitation of the products, and $D(Ar\text{-}D^+)$ is the dissociation energy of ArD^+ to Ar and D^+. The range of possible values of Q is limited by the value of ΔE_o^o, and the requirement that $U \leq D$ for the product to be stable in its ground electronic state. Thus

$$-2.3 \leq Q \leq -\Delta E_o^o$$

The value of ΔE_o^o is not known. However, analogy to the isoelectronic HCl molecule suggests that $D(Ar^+\text{-}D)$ may be as great as 4.4 eV, and thus that $D(Ar\text{-}D^+)$ could be as large as 3.3 eV. This would give a value of -1 eV for ΔE_o^o, and an approximate upper limit for Q of +1 eV.

The approximate limits for Q are indicated in Figs. 1 and 4. Product is found throughout the allowed range of Q, and in parts of the regions excluded by the product stability and conservation of energy criteria. This scattering into the forbidden regions can be explained qualitatively by consideration of the motion of the target gas and of the finite resolution of the apparatus.

Introduction of the limits on the allowed values of Q leads to a rationalization of why the intensity maximum for forward scattered products moves to velocities greater than the ideal stripping velocity as the initial relative energy

is raised above 4.5 eV. As Fig. 4 shows, for collisions at 4.55 eV, products having the stripping velocity are excited internally nearly to their dissociation limit. For higher initial relative energies, the stripping velocity lies in the region forbidden by product instability. At these higher relative energies, forward recoil to speeds in excess of the stripping velocity is necessary if stable products are to be formed. The same explanation has been used[3] to explain the very similar behavior found for the products of the $N_2^+(D_2,D)N_2D^+$ reaction.

While the combination of product recoil and small or zero deflection may seem incompatible, it can arise if the potential energy surface is such that the reactants are attracted to each other on the incoming leg of the trajectory, and the products are repelled from each other on the outgoing leg. The respective negative and positive contributions to the deflection angle will tend to cancel, and produce small angle scattering with acceleration of the products above the ideal stripping velocity. It seems very unlikely that a potential energy surface which assumes only attractive forces between reactants and between products could produce the strong peaking of the product at small barycentric angles since the contributions to the deflection angle from the incoming and outgoing legs of the trajectory would add to give scattering through a substantial angle. It also could not explain the product stabilization that occurs at high energies. A surface which assumes

repulsion between products, and small or zero repulsion between reactants could also lead to products accelerated beyond the ideal stripping velocity, but again would not produce peaking at zero degrees if the product repulsion were large enough to stabilize the product. Only if the repulsion occurred rather late in the course of the collision and was therefore directed along the zero degree line could this potential produce recoil and zero degree scattering. The combination of reactant attraction and product repulsion seems easier to accept.

Examination of the original plots of product intensity as a function of laboratory energy as well as Table I shows that with one exception, when the initial relative energy is less than 7 eV, the Q values for products scattered through large angles are somewhat greater than those for forward scattered products. This indicates that the products of rebound or small impact parameter collisions (in which the three atoms must interact strongly) are less excited internally than are the products of grazing collisions. A similar observation was made for the N_2^+-D_2 system.[3] However, for initial relative energies above 7 eV, the back and forward scattered products of the $Ar^+(D_2,D)ArD^+$ reaction both appear to be excited to levels very near to their dissociation limit. Although the resolution of our apparatus permits only this qualitative assessment of product internal excitation at these higher collision energies, it does appear that difficulty in forming molecular ions which are stable to dissociation is a major

factor which limits the partial cross sections for both back and forward scattered products.

Among the more interesting observations drawn from a comparison of the intensity contour maps in the surprising prevelence of nonreactive scattering of Ar^+ by D_2, and the striking resemblance of its distribution to that of Ar^+ scattered by He for the same initial relative energy. The intensity of Ar^+ scattered nonreactively from D_2 is particularly surprising, since the very large reaction rate constant that has been measured[6] at relative energies less than 1 eV is consistent with the assumption that reaction occurs upon every close collision. Apparently at these higher energies it is possible even for head-on collisions between Ar^+ and D_2 to occur, and produce no reaction in a majority of cases. This is in marked contrast to the N_2^+-D_2 system,[3] where very little nonreactively scattered N_2^+ was detected.

The similarity of the distributions of Ar^+ scattered from D_2 and He leads to the surprising conclusion that most Ar^+ is scattered by D_2 elastically, or at best only slightly inelastically. Although general considerations,[16] and as well, the classical calculations of Wolfsberg and Kelly[17] show that the combination of a heavy projectile impinging on an oscillator composed of two light atoms does not favor excitation of the oscillator, the strong interactions in the potentially reactive Ar^+-D_2 system might be expected to lead to substantial vibrational excitation of D_2. Indeed, the nonreactive scattering in the O_2^+-D_2 system is extremely inelastic,[18] and the

small amount of nonreactive scattering of N_2^+ by D_2 is also largely inelastic.[3] However, Figs. 2 and 5 indicate that in most nonreactive Ar^+-D_2 collisions, the D_2 is left with less than 0.5 eV internal energy. Other maps which we do not publish here show that this is true even when the initial relative energy of collision is as high as 12.1 eV. The experiments of Dittner and Datz[19] show a similarly small vibrational excitation of D_2 by collisions of K^+ and K with D_2 in the same range of energies.

The most primitive analysis of collisional vibrational excitation shows that it occurs because interaction potential between the atomic projectile and the target diatomic is a function of both the projectile-target distance and the internuclear distance of the molecule. Our results, which show that the nonreactive scattering is first of all intense and second quite elastic, indicate that in this high energy regime the ion-molecule potential is not very sensitive to the internuclear distance in the molecule.

To compare the reactive and nonreactive scattering further, it is advantageous to have available product angular distributions or differential cross sections. Accordingly, for each of the twelve velocity vector maps we have integrated the specific intensity over the barycentric velocity at a series of angles spaced by twenty degree intervals. The resulting set of twelve relative differential cross sections was put on an absolute basis by integrating the reactive cross sections

over angle to give relative total reaction cross sections, and then normalizing our result from the 2.77 eV experiment to the absolute total reaction cross section determined by Robb et al.[20] for the same energy.

Figure 7 shows the twelve absolute differential cross sections. At each energy, the Ar^+ scattered nonreactively from D_2 has an angular distribution that is somewhat smaller and shaped very similarly to the differential cross section for Ar^+-He scattering. This result is rather different from the observations by Greene et al.[21] of the nonreactive scattering of potassium atoms from hydrogen halides and krypton. In these systems, the nonreactive scattering of K and HX is noticeably attenuated at large scattering angles, but is similar to scattering of K by a rare gas at small angles. This indicates that small impact parameter collisions are necessary if reaction is to occur. Our results in Fig. 7 show no such features, and consequently we conclude that the reaction probability is not sensitively dependent on impact parameter for values of the impact parameter less than approximately 2 Å.

For the 2.75, 6.83, and 9.13 eV experiments, the differential reaction cross section is less than the nonreactive cross section at all angles. For the 2.75 and 6.83 eV experiments, the sum of the reactive and nonreactive Ar^+-D_2 cross sections closely approximates the Ar^+-He differential cross section at angles greater than 60°. This approximate relation is not unexpected, in view of the fact that the reactive and

nonreactive scattering at large angles involves the repulsive potentials of Ar^+ with D_2 and He, which are likely to be of similar form and magnitude. The discrepancy between the sum of the reactive and nonreactive scattering from D_2 and the scattering from He that is apparent in the 9.13 eV experiment is probably due to the increased importance of dissociative and nondissociative charge transfer from Ar^+ to D_2 at these higher energies.

The 4.55 eV experiment is unique in showing an Ar^+-D_2 reactive differential cross section larger than the nonreactive cross section. It is likely that this is a consquence of some systematic experimental error in this one reactive experiment, although we have been unable to identify a highly probable cause. The total reaction cross section found at this energy exceeds by a factor of 1.7 the value interpolated linearly from a plot of ln σ as a function of energy, and thus it seems probable that both the total and differential cross sections are in error by approximately this factor at 4.55 eV.

The similarity between the sum of the Ar^+-D_2 reactive and elastic cross sections and the Ar^+-He differential cross section suggest that we might define a reaction probability $P(\theta)$ at each angle by

$$P(\theta) = I_{ArD^+}(\theta)/I_{Ar^+\text{-He}}(\theta)$$

or by replacing the denominator by the sum of the Ar^+-D_2 reactive and elastic differential cross sections. The quantity $P(\theta)$ is not necessarily simply related to the more interesting quantity $P(b)$, where b is the impact parameter, since in general

reactive and nonreactive collisions with the same impact parameter do not give products at the same angle. However, $P(\theta=\pi)$ is very probably the same as $P(b=0)$ for these high energy collisions. Evaluation of these reaction probabilities for head-on collisions show that their averages range from approximately 0.1 at 9.13 eV up to 0.35 at 2.77 eV. Thus while the assumption that "close" or head-on collisions always lead to reaction is surely not correct in this higher energy range, it becomes increasingly appropriate as the relative energy decreases. Extrapolation of our reaction probabilities to relative energies below 1 eV suggests that reaction at nearly every close collision is an accurate description at such low energies.

In the course of determining and working with the differential scattering cross sections, it became clear that the unfavorable Ar^+/D_2 mass ratio had produced a resolution in the center of mass system that was low enough to affect seriously the appearance of the calculated differential cross section. This instrumental broadening does not falsify our qualitative comparison of reactive and nonreactive scattering by particles of the same mass measured on the same apparatus. However, to remove the effects of apparatus smearing, and to make the comparison of the results of several laboratories more meaningful, we have attempted a partial deconvolution of the reactive scattering angular distributions. This analysis follows.

We first obtain an equation which relates the measured specific intensity of product to the spread in $\underset{\sim}{v}_i$, the initial beam velocity, and the detector band pass. If $N(\underset{\sim}{v}_i,\underset{\sim}{v})$ is the flux of product (particles/sec per unit velocity space volume), $N^o(\underset{\sim}{v}_i)$ the flux of primary beam particles, ρ is the scattering gas density and ℓ the scattering length, the specific intensity of product $I(\underset{\sim}{v}_i,\underset{\sim}{v})$ is defined by

$$N(\underset{\sim}{v}_i,\underset{\sim}{v}) = I(\underset{\sim}{v}_i,\underset{\sim}{v})\, N^o(\underset{\sim}{v}_i)\, \rho\ell \qquad (1)$$

We assume that the scattering gas is at rest, and thus $\underset{\sim}{v}_i$ is the initial relative velocity. To obtain the number of products counted by the detector per second, we must integrate $N(\underset{\sim}{v}_i,\underset{\sim}{v})$ over the properly normalized beam distribution and detector band pass functions. Accordingly we define $P(\underset{\sim}{v}_i)$, the normalized velocity vector distribution function for the primary beam by

$$N^o(\underset{\sim}{v}_i) = I^o\, P(\underset{\sim}{v}_i) \qquad (2)$$

where $I^o(\underset{\sim}{v}_o)$ is the total beam current of nominal velocity $\underset{\sim}{v}_o$. Also, we define the detector band pass function $B(\underset{\sim}{v}_D,\underset{\sim}{v})$ as the probability that a particle with $\underset{\sim}{v}$ will be counted when the detector is set at $\underset{\sim}{v}_D$. Integration of $B(\underset{\sim}{v}_D,\underset{\sim}{v})$ over all velocity space gives Z, the nominal volume in velocity space intercepted by the detector:

$$\int B(\underset{\sim}{v}_D,\underset{\sim}{v})\, d\underset{\sim}{v} = Z \qquad (3)$$

Substitution of Eq. (2) in (1), multiplication by $B(\underset{\sim}{v}_D,\underset{\sim}{v})$ and integration over all values of $\underset{\sim}{v}$ and $\underset{\sim}{v}_i$ gives C, the total number of counts per second at a detector set at $\underset{\sim}{v}_D$:

$$C = \int N(\underset{\sim}{v}_i, \underset{\sim}{v})\ B(\underset{\sim}{v}_D, \underset{\sim}{v})\ d\underset{\sim}{v}\ d\underset{\sim}{v}_i$$

$$= \rho \ell\ I^o \int P(\underset{\sim}{v}_i)\ d\underset{\sim}{v}_i \int I(\underset{\sim}{v}_i, \underset{\sim}{v})\ B(\underset{\sim}{v}_D, \underset{\sim}{v})\ d\underset{\sim}{v}$$

$$= \rho \ell\ I^o\ Z\ \bar{I}(\underset{\sim}{v}_o, \underset{\sim}{v}_D)$$

The last equality defines $\bar{I}(\underset{\sim}{v}_o, \underset{\sim}{v}_D)$, the specific intensity averaged over the detector volume and beam distribution. It is equal to the true specific intensity $I(\underset{\sim}{v}_o, \underset{\sim}{v}_D)$ in the limit of ideal apparatus resolution, or when $I(\underset{\sim}{v}_o, \underset{\sim}{v}_D)$ varies only infinitesimally over the detector volume and beam distribution.

We have previously shown[3] that $I(\underset{\sim}{v}_i, \underset{\sim}{v})$ is equal to $I(\underset{\sim}{v}_i, \underset{\sim}{u})$, where $\underset{\sim}{u}$ is the product velocity in the center of mass system. It is easy to show from this and the equality of volume elements in the laboratory and barycentric systems that

$$\bar{I}(\underset{\sim}{v}_o, \underset{\sim}{v}_D) = \int P(v_i) d\underset{\sim}{v}_i \int B(\underset{\sim}{v}_D, \underset{\sim}{v})\ I(\underset{\sim}{v}_i, \underset{\sim}{v})\ d\underset{\sim}{v}/Z \qquad (4)$$

$$= \int P(v_i) d\underset{\sim}{v}_i \int B(\underset{\sim}{u}_D, \underset{\sim}{u})\ I(\underset{\sim}{v}_i, \underset{\sim}{u})\ d\underset{\sim}{u}/Z$$

$$= \bar{I}(\underset{\sim}{v}_o, \underset{\sim}{u}_D)$$

The latter quantity is what we have plotted in Figs. 1-6, and in all our previous work. The experimental differential and total cross sections can be calculated as follows:

$$\bar{I}_{lab}(\Theta_D) = \int_0^\infty \bar{I}(\underset{\sim}{v}_o, \underset{\sim}{v}_D) v_D^2\ dv_D$$

$$\bar{I}_{CM}(\theta_D) = \int_0^\infty \bar{I}(\underset{\sim}{v}_o, \underset{\sim}{u}_D)\ u_D^2 du_D$$

$$\bar{\sigma} = 2\pi \int_0^{\pi} \sin\Theta_D \, \bar{I}(\Theta_D) \, d\Theta_D$$

$$= 2\pi \int_0^{\pi} \sin\theta_D \, I(\theta_D) \, d\theta$$

If there is appreciable apparatus smearing, none of these quantities is equal to its true value.

We will estimate the effect of finite apparatus resolution on $I(\theta)$ at small angles by assuming simple Gaussian forms for $I(\underset{\sim}{v}_i,\underset{\sim}{u})$, $P(\underset{\sim}{v}_i)$, and $B(\underset{\sim}{v}_D,\underset{\sim}{v})$, and using Eq. (4). The coordinate system and the important angles are shown in Fig. 8, where the z-axis is taken to lie along v_o, and the detector is assumed to be located above the positive x-axis. Since $I(\underset{\sim}{v}_i,\underset{\sim}{v})$ depends on the angle Θ between $\underset{\sim}{v}_i$ and $\underset{\sim}{v}$, and $B(\underset{\sim}{v}_D,\underset{\sim}{v})$ is a function of the angle Θ_{fD} between $\underset{\sim}{v}_D$ and $\underset{\sim}{v}$, we must express Θ and Θ_{fD} in terms of Θ_f, Θ_i, and Θ_D. This can be done by using the spherical harmonic addition theorem, which in the limit of the very small angles we are interested in gives

$$\Theta^2 = \Theta_f^2 + \Theta_i^2 - 2\Theta_f \, \Theta_i \cos(\Phi_f - \Phi_i)$$

$$\Theta_{fD}^2 = \Theta_f^2 + \Theta_D^2 - 2\Theta_f\Theta_D \cos \Phi_f$$

For simplicity, we assume $P(\underset{\sim}{v}_i)$ and $B(\underset{\sim}{v}_D,\underset{\sim}{v})$ can each be expressed as a Gaussian function of angle times a Gaussian function of speed. The appropriate functions are

$$P(\underset{\sim}{v}_i) = \left[\pi^{3/2}(\Delta v_i)(\Delta\Theta_i)v_i^2\right]^{-1} \exp\left[-(\Theta_i/\Delta\Theta_i)^2\right] \exp\left[-(v_i-v_o)^2/(\Delta v_i)^2\right] \tag{5}$$

$$B(\underset{\sim}{v}_D,\underset{\sim}{v}) = Z\left[\pi^{3/2}(\Delta v_D)(\Delta\Theta_D)^2 v_D^2\right]^{-1} \exp\left[-(\Theta_{fD}/\Delta\Theta_D)^2\right] \exp\left[-(v-v_D)^2/(\Delta v_o)^2\right] \tag{6}$$

and are normalized as indicated earlier, under the assumptions that $\Delta v_i << v_o$, and $\Delta\Theta_i << 1$.

Inspection of the ArD^+ distributions suggests that the barycentric differential cross section can be expressed as the sum of two contributions, one a term strongly peaked at θ equal to zero, and a second, slowly varying term, which contributes a small amount at all barycentric angles, somewhat like hard sphere scattering. For the sharply peaked, or stripping, term we assume a product of Gaussian functions of angle and speed. Thus

$$I(\underset{\sim}{v}_i,\underset{\sim}{u}) = \sigma_{st}\left[\pi^{3/2}(\Delta u_f)(\Delta\theta_f)^2 u^2\right]^{-1} \exp\left[-(\theta/\Delta\theta_f)^2\right] \exp\left[-(u-bu_i)^2/(\Delta u_f)^2\right] + I_{HS}(\underset{\sim}{v}_i,\underset{\sim}{u}) \tag{7}$$

Assuming that the first term is strongly peaked, we get

$$\sigma = \int I(\underset{\sim}{v}_i,\underset{\sim}{u})\, d\underset{\sim}{u} = \sigma_{st} + \sigma_{HS}.$$

That is, the total cross section is the sum of a "stripping" plus a "hard sphere" cross section. We shall assume I_{HS} is not appreciably distorted by apparatus resolution. The first term, however, must be transformed into the laboratory coordinates,

and substituted in Eq. (4) to determine the effect of apparatus resolution.

In Eq. (7) we have assumed that the final barycentric velocity peaks at a fixed fraction b of the initial velocity u_i. Consequently, if the target is at rest, the final laboratory velocity peaks at av_i where

$$a = b + (1-b)M_1/(M_1 + M_2)$$

and M_1 and M_2 are respectively the projectile and target masses.

Under the assumption that the stripping function is sharply peaked in angle, we use

$$\theta = (av_i)\,\Theta/(bu_i)$$

and perform the straightforward transformation of $I(\underset{\sim}{v}_i, \underset{\sim}{u})$ to $I(\underset{\sim}{v}_i, \underset{\sim}{v})$ to get

$$I(\underset{\sim}{v}_i, \underset{\sim}{v}) = \sigma_{st}\left[\pi^{3/2}(\Delta v_f)(\Delta\Theta_f)^2(v-v_c)^2(av_i)^2/(bu_i)^2\right]^{-1}$$
$$\exp\left[-(\Theta/\Delta\Theta_f)^2\right] \times \exp\left[-(v-av_i)^2/(\Delta v_f)^2\right]$$
$$+ I_{HS}(\underset{\sim}{v}_i, \underset{\sim}{v}) \qquad (8)$$

with

$$\Delta v_f = \Delta u_f,\ \Delta\Theta_f = (bu_i)\Delta\theta_f/(av_i),\ v_c = M_1 v_i/(M_1+M_2)$$

The final results for the experimental specific intensity $\bar{I}(\underset{\sim}{v}_o, \underset{\sim}{v}_D)$, the experimental differential cross section $\bar{I}(\Theta_D)$, and the experimental total cross sections are obtained by substituting Eqs. (5), (6), and (8) in (4). We obtain

$$\bar{I}(\underset{\sim}{v}_o,\underset{\sim}{v}_D) = I_{HS}(\underset{\sim}{v}_o,\underset{\sim}{v}_D) + \sigma_{st}(\pi)^{-3/2}\left[\Delta\Theta_i^2 + \Delta\Theta_f^2 + \Delta\Theta_D^2\right]^{-1}$$

$$\left[a^2\Delta v_i^2 + \Delta v_f^2 + \Delta v_D^2\right]^{-1} \cdot v_D^{-2} \exp\left[-(\Theta_D)^2/(\Delta\Theta_i^2 + \Delta\Theta_f^2 + \Delta\Theta_D^2)\right]$$

$$\exp\left[-(v_D - av_o)^2/(a^2\Delta v_i^2 + \Delta v_f^2 + \Delta v_D^2)\right] \qquad (9)$$

$$\bar{I}(\Theta_D) = I_{HS}(\Theta_D) + (\sigma_{st}/\pi)\left[\Delta\Theta_i^2 + \Delta\Theta_f^2 + \Delta\Theta_D^2\right]^{-1}$$

$$\exp\left[-\Theta_D^2/(\Delta\Theta_i^2 + \Delta\Theta_f^2 + \Delta\Theta_D^2)\right] \qquad (10)$$

$$\bar{\sigma} = \sigma_{HS} + \sigma_{st} = \sigma. \qquad (11)$$

Thus in this case the experimental total cross section equals the true value. The experimental barycentric distribution follows from the equality of $\bar{I}(\underset{\sim}{v}_o,\underset{\sim}{v}_D)$ and $\bar{I}(\underset{\sim}{v}_o,\underset{\sim}{u}_D)$ and integration over velocity. The result is

$$\bar{I}(\theta_D) = I_{HS}(\theta_D) + (\sigma_{st}/\pi)\left[(\Delta\theta_i)^2 + (\Delta\theta_f)^2 + (\Delta\theta_D)^2\right]^{-1}$$

$$\exp\left\{-\theta_D^2/\left[(\Delta\theta_i)^2 + (\Delta\theta_f)^2 + (\Delta\theta_D)^2\right]\right\} \qquad (12)$$

Here all the barycentric distribution parameters $\Delta\theta$ are related to their laboratory counterparts by

$$\Delta\theta = (av_o/bu_o)\,\Delta\Theta \qquad (13)$$

Equation (12) represents the experimentally determined differential reaction cross section. From the measured angular shape of the unscattered ion beam, we could determine the sum of the squares of $\Delta\theta_i$ and $\Delta\theta_D$. Thus by fitting our data to a form resembling Eq. (12), and making use of the Gaussian

parameters of the beam and detector, we could deduce $\Delta\theta_f$, and thus the "true" differential scattering cross section

$$I(\theta_D) = I_{HS}(\theta_D) + (\sigma_{st}/\pi)(\Delta\theta_f)^{-2} \exp\left[-\theta_D^2/(\Delta\theta_f)^2\right] \quad (14)$$

The experimental differential cross sections for the $Ar^+(D_2,D)ArD^+$, $N_2^+(D_2,D)N_2D^+$, and $N_2^+(H_2,H)N_2H^+$ reactions were fit to the form

$$I(\theta_D) = A \exp[-(\theta/\alpha)^2] + B + C\, P_2(\cos\theta) \quad (15)$$

where $P_2(\cos\theta)$ is the Legendre polynomial, using the least squares criterion of minimizing

$$S = \sum_{data} \left[I_{exp}(\theta_D) - I_{calc}(\theta_D)\right]^2/\left[I_{exp}(\theta_D)\right]^2$$

The experimental $\overline{I}(\theta_D)$ were evaluated at 20° increments, so ten points were available for the fit in each experiment. The RMS deviations for the various fits averaged 8%. Other forms in which the first two terms of Eq. (15) alone or with $P_1(\cos\theta)$ were tried, but could be fit somewhat less successfully.

From the parameters of the analytical fit to the experimental data, it is possible to calculate the parts of the total cross section associated with "hard sphere" and with "stripping" which are given respectively by

$$\sigma_{HS} = 4\pi B$$

$$\sigma_{st} = \pi A\alpha^2\left[1 - \frac{\alpha^2}{3!} + \frac{2\alpha^4}{5!} - \frac{6\alpha^6}{7!} + \cdots\right]$$

The stripping fraction $\sigma_{st}/(\sigma_{st} + \sigma_{HS})$ was calculated for each experiment, and the values are given in Table II, along with the measured beam width

$$\Delta\theta_B = \left[(\Delta\theta_i)^2 + (\Delta\theta_D)^2\right]^{1/2}$$

and the true scattering width

$$\Delta\theta_f = (\alpha^2 - \Delta\theta_B^2)^{1/2}$$

The true $I(\theta_D)$ was estimated for all the experiments by replacing α in Eq. (15) by $\Delta\theta_f$, and increasing A to A' in order to keep σ_{st} constant. The ratios A'/A are also given in Table II. A similar analysis of the results of this laboratory[3] on the N_2^+-D_2, and N_2^+-H_2 reaction was also performed, and the results are also presented in Table II.

Examination of Table II shows that the stripping fraction for the Ar^+-D_2 reaction falls rapidly with increasing relative energy. This indicates that as the relative energy increases, it becomes increasingly difficult to obtain from grazing collisions products that are stable to dissociation. This effect is not evident for the reactions of N_2^+ with H_2 and D_2 in spite of the earlier conclusion,[22] drawn from a qualitative examination of the scattering maps, that it did occur in this system. Apparently the differences in masses and in the potential energy surfaces is sufficient so that stabilization of the products is less of a problem in the N_2^+ reactions than in the Ar^+-D_2 system. This would be the case if the repulsion between the ArD^+ and D products was somewhat less than that

between N_2D^+ and D. This would explain the somewhat sharper angular distribution of ArD^+ compared to that of N_2D^+ which we shall discuss below. In addition, it may be a partial explanation of the fact that the total cross section for the N_2^+-D_2 reaction exceeds that for the Ar^+-D_2 reaction.

A closer comparison of the Ar^+-D_2 and N_2^+-D_2 systems is given in Fig. 9. Here the deconvoluted ratio $I(\theta_D)/I(0)$ is plotted for the ion-molecule systems and for the $K(Cl_2,Cl)KCl$ reaction,[23] which is probably the most strongly forward peaked of the alkali metal reactions so far studied. The comparison shows how very sharply peaked the ion-molecule reactions are, especially at the higher relative energies. Even so, none of these reactive systems give scattering as sharply peaked as that found for the $N_2^+ + CH_4$, CD_4 systems which we studied earlier.[4] The deconvoluted scattering widths for these systems are only four or five degrees.

A second difference between the Ar^+-D_2 and N_2^+-D_2 system is evident in Fig. 9. The width of the stripping peak for the Ar^+-D_2 reaction is virtually the same at the energies studied in this work. In contrast, the breadth of the N_2D^+ product peak increases noticeably at the lower energies. When the data from other laboratories is examined, however, the difference between the two systems is less marked. We have analyzed the laboratory differential cross sections measured in the work of Wolfgang,[14] Turner,[24] and Bailey,[13] fitting them by means of Eq. (10) and assuming that the hard sphere

contribution can be neglected at small angles. The effect of the beam width $\Delta\Theta_B$ was taken into account[25] by combining it with the measured product width $\Delta\Theta$ to give a "true" scattering width

$$\Delta\Theta_f = \left[(\Delta\Theta)^2 - (\Delta\Theta_B)^2\right]^{1/2}$$

Finally the center of mass scattering width was computed using Eq. (13) and the ratio of v/u at the intensity maximum. Thus, aside from the neglect of the contribution of product scattered through large barycentric angle, our treatment of the data from these other laboratories involves no new assumptions and approximations.

The resultant values of $\Delta\theta_f$ are shown in Fig. 10. The agreement between our work, and that of Wolfgang et al.[14] and Turner et al.[24] is remarkably good. The work of Bailey et al.[13] appears to be 25% lower in the case of N_2D^+ and 25% higher for ArD^+ than the results of others, but in both cases has the energy dependence found in the other laboratories. It should be understood that the approximations which we have used break down badly at low energies where the scattering is neither sharply peaked in angle, nor well separated from the center of mass. Consequently, we have not included Wolfgang's lowest energy data in the analysis.

From Fig. 10 we see that the scattering width for N_2D^+ is greater, and falls more slowly with increasing energy than does the scattering width for ArD^+. The widths for N_2H^+

N_2D^+ are the same at the same relative energies, which suggests the widths are determined more by the potential energy surface than by the masses of reactants. Furthermore, the differences between the N_2^+-D_2 and Ar^+-D_2 systems even at low energies show that factors more complicated than the simple ion-induced dipole potential determine the distribution of small angle scattering.

SUMMARY

From our product velocity vector distributions we have demonstrated that the $Ar^+(D_2,D)ArD^+$ reaction proceeds by a direct interaction, at least for initial relative energies above 2.27 eV. The most probable reactive process produces ArD^+ moving in the original direction of the Ar^+ projectile, although products are scattered with appreciable intensity through the complete range of barycentric angles, even at relative energies as low as 2.27 eV. The nonreactive scattering of Ar^+ by D_2 is surprisingly intense, is predominantly elastic or only slightly inelastic, and closely resembles the scattering of Ar^+ by He. The reaction probability at a particular energy is essentially constant for scattering angles greater than 60°, and increases as the initial energy decreases. Partial deconvolution of the differential reactive scattering cross sections shows that the ArD^+ has an angular distribution more sharply forward peaked than any other known reactive differential cross section for systems of four atoms or less. The partial

cross section for stripping or forward scattering falls as the initial reactive energy increases, and accounts for less than half of the total reactive scattering at the higher energies. The true scattering widths for $Ar^+(D_2,D)ArD^+$ and $N_2^+(D_2,D)N_2D^+$ deduced from the data of several laboratories are in surprisingly good agreement, and along with our measurements of the nonreactive scattering in both systems, show that there are clear differences in the dynamics of these two apparently similar reactions.

Acknowledgements.- This work was supported by the U.S. Atomic Energy Commission. E.A.G. acknowledges a postdoctoral fellowship from the National Center for Air Pollution Control of the Public Health Service.

Table I. Scattering data for reactive $Ar^+(D_2,D)ArD^+$ Experiments.

E_{rel} (eV)	v_o x10^{-5} (cm/sec)	Forward Peak		Backward Peak	
		v_f/v_o [a]	Q [b] (eV)	v_f/v_o	Q [b] (eV)
2.26	10.959	0.9609	-0.70	0.8734	(-1.55)
2.73 [c]	12.033	0.9563	-1.18	0.8543	-0.64
3.63	13.880	0.9542	-1.75	0.8619	-1.57
4.55	15.545	0.9547	-2.13	0.8577	-1.50
4.55 [c]	15.544	0.9555	-2.06	0.8589	-1.63
5.48	17.056	0.9568	-2.31	0.8551	-1.42
6.78	18.980	0.9605	-2.23	0.8592	-2.49
6.78	18.982	0.9594	-2.42	0.8551	-1.75
8.12	20.776	--	$\leq$-2.0	0.8571	-2.54
9.01	21.990	--	$\leq$-2.0	0.8527	-1.74
9.14	22.043	--	$\leq$-2.0	0.8553	-2.41

a. v_f is the velocity of the scattering peaks at zero laboratory degrees and v_o is the initial ion beam velocity. For ideal stripping, v_f/v_o = 0.9524.

b. Experimental uncertainty in Q is $\pm$ 0.15 eV for forward peak, $\pm$ 0.35 eV for the broader backward peak. The location of the backward peak at 2.26 eV relative energy is very uncertain.

c. Complete contour maps shown in text.

Table II. Parameters for deconvolution of Ar^+-D_2 and N_2^+-(H_2,D_2) Reactive Scattering.

Reaction	E_{rel}	$\Delta\theta_B$ (deg)	$\Delta\theta_f$ (deg)	$\sigma_{(st)}/\sigma_{(total)}$	A'/A
Ar^+-D_2	2.72	35.6	29	0.54	2.71
	4.54	14.4	26	0.38	1.22
	4.54	20.9	30	0.40	1.82
	6.83	17.0	29	0.17	1.55
N_2^+-D_2	3.12	21.8	50	0.63	1.18
	8.12	10.8	34	0.53	1.11
	11.23	15.5	27	0.58	1.30
N_2^+-H_2	3.13	31.5	53	0.50	1.32
	5.62	25.4	36	0.59	1.45
	8.11	28.3	36	0.46	1.57

References

1. W. R. Gentry, E. A. Gislason, Y. T. Lee, B. H. Mahan, and C. W. Tsao, Disc. Faraday Soc. 44, 137 (1967).
2. W. R. Gentry, E. A. Gislason, B. H. Mahan, and C. W. Tsao, J. Chem. Phys. 47, 1856 (1967).
3. W. R. Gentry, E. A. Gislason, B. H. Mahan, and C. W. Tsao, J. Chem. Phys. 49, 3058 (1968).
4. E. A. Gislason, B. H. Mahan, C. W. Tsao, and A. S. Werner, J. Chem. Phys. 50, 142 (1969).
5. E. A. Gislason, B. H. Mahan, C. W. Tsao, and A. S. Werner, J. Chem. Phys. 50, 5418 (1969).
6. D. P. Stevenson and D. O. Schissler, J. Chem. Phys. 29, 292 (1958).
7. F. S. Klein and L. Friedman, J. Chem. Phys. 41, 1789 (1964).
8. C. F. Giese and W. B. Maier II, J. Chem. Phys. 39, 739 (1963).
9. K. Lacmann and A. Henglein, Ber. Bunsenges. Phys. Chem. 69, 286 (1965).
10. A. Henglein, K. Lacmann, and B. Knoll, J. Chem. Phys. 43, 1048 (1965).
11. A. Ding, K. Lacmann, and A. Henglein, Ber. Bunsenges. Phys. Chem. 71, 596 (1967).
12. R. D. Fink and J. S. King, Jr., J. Chem. Phys. 47, 1857 (1967).
13. L. D. Doverspike, R. L. Champion, and T. L. Bailey, J. Chem. Phys. 45, 4385 (1966).

References (Continued)

14. Z. Herman, J. Kerstetter, T. Rose, and R. Wolfgang, Disc. Faraday Soc. 44, 123 (1967).

15. R. Wolfgang and R. J. Cross, Jr., J. Phys. Chem. 73, 743 (1969).

16. D. Rapp and T. Kassal, Chem. Rev. 69, 61 (1969).

17. J. D. Kelley and M. Wolfsberg, J. Chem. Phys. 44, 324 (1966).

18. Unpublished results of this laboratory.

19. (a) P. F. Dittner and S. Datz, J. Chem. Phys. 49, 1969 (1968); (b) Abs. Sixth Int. Conf. on Physics of Elec. and Atomic Collisions, Cambridge, Mass., 1969, p. 469.

20. J. B. Homer, R. S. Lehrle, J. C. Robb, and D. W. Thomas, Nature 202, 795 (1964).

21. E. F. Greene, A. L. Moursund, and J. Ross, Adv. Chem. Physics. X (J. Wiley and Sons, Inc., New York, 1966), p. 135.

22. B. H. Mahan, Accounts of Chem. Res. 1, 217 (1968).

23. R. Grice and P. Empedocles, J. Chem. Phys. 48, 5352 (1968).

24. B. R. Turner, M. A. Fineman, and R. F. Stebbings, J. Chem. Phys. 42, 4088 (1965).

25. In the low energy experiments of Wolfgang et al.[14] the velocity of the target gas is comparable to the velocity of the ions, and adds an additional width to the scattering. However, the predicted ideal stripping product profile plotted in Wolfgang's paper is just the convolution of the ion velocity with the target velocity which is the quantity needed to find $\Delta\Theta_f$ from $\Delta\Theta$. Turner et al.[23] give beam widths only for their two lowest energies. We have assumed that the beam width is the same (1.19°) at all other energies.

Figure Captions

Fig. 1. A contour map of the intensity of ArD^+ per unit velocity space volume (the specific intensity of ArD^+) in the center of mass coordinate system. The circles labeled Q = +1.0 eV and -2.5 eV enclose the approximate region of velocity space allowed by the reaction exothermicity and product stability, respectively, for scattering of an infinitely sharp beam from the stationary target. The cross near the intensity peak locates the ideal stripping velocity.

Fig. 2. A contour map of the normalized specific intensity in the center of mass coordinate system of Ar^+ scattered nonreactively from D_2. The circle through the beam intensity maximum is the locus of elastic scattering.

Fig. 3. A contour map of the specific intensity of Ar^+ scattered by He. The circle labeled Q = 0 locates the elastic scattering of an infinitely sharp beam from a stationary target. The intensity units are such that the intensities in all maps in this article may be compared directly.

Fig. 4. A contour map of the specific intensity of ArD^+. The cross near the intensity peak locates the ideal stripping velocity.

Figure Captions (Continued)

Fig. 5. A contour map of the specific intensity of Ar^+ scattered nonreactively from D_2.

Fig. 6. A contour map of the specific intensity of Ar^+ scattered nonreactively from He.

Fig. 7. The absolute barycentric differential scattering cross sections for reactive and nonreactive scattering of Ar^+ by D_2 and He in units of square angstroms per steradian. The dashed line in the upper two panels represents the sum of the reactive and nonreactive scattering in the Ar^+-D_2 system.

Fig. 8. The velocity vector diagram used in the approximate deconvolution procedure.

Fig. 9. A comparison of several differential reaction cross sections after the approximate deconvolution. Note the different ordinate for Ar^+-D_2 and the other reactions.

Fig. 10. A comparison of the dependence of the gaussian width of the small angle scattering on relative energies for three ion-molecule reactions from four laboratories. In the lower panel, the symbols refer to the Ar^+-D_2 reaction, and the curve represents the N_2^+-D_2 reaction.

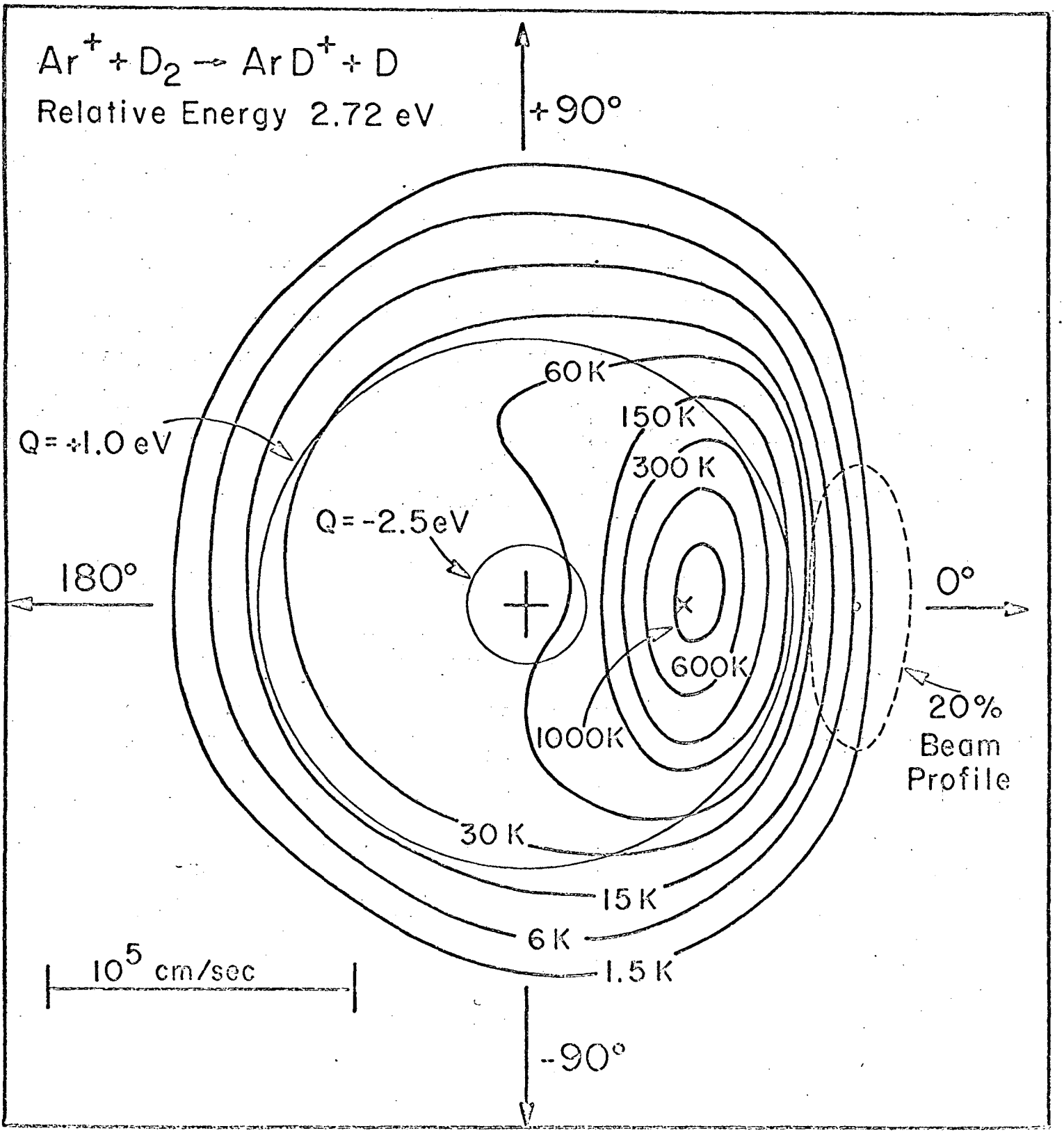
$Ar^+ + D_2 \rightarrow ArD^+ + D$
Relative Energy 2.72 eV
+90°
60 K
150 K
300 K
600K
1000K
Q = +1.0 eV
Q = -2.5eV
180°
0°
20% Beam Profile
30 K
15 K
6 K
1.5 K
10^5 cm/sec
-90°

Fig.1

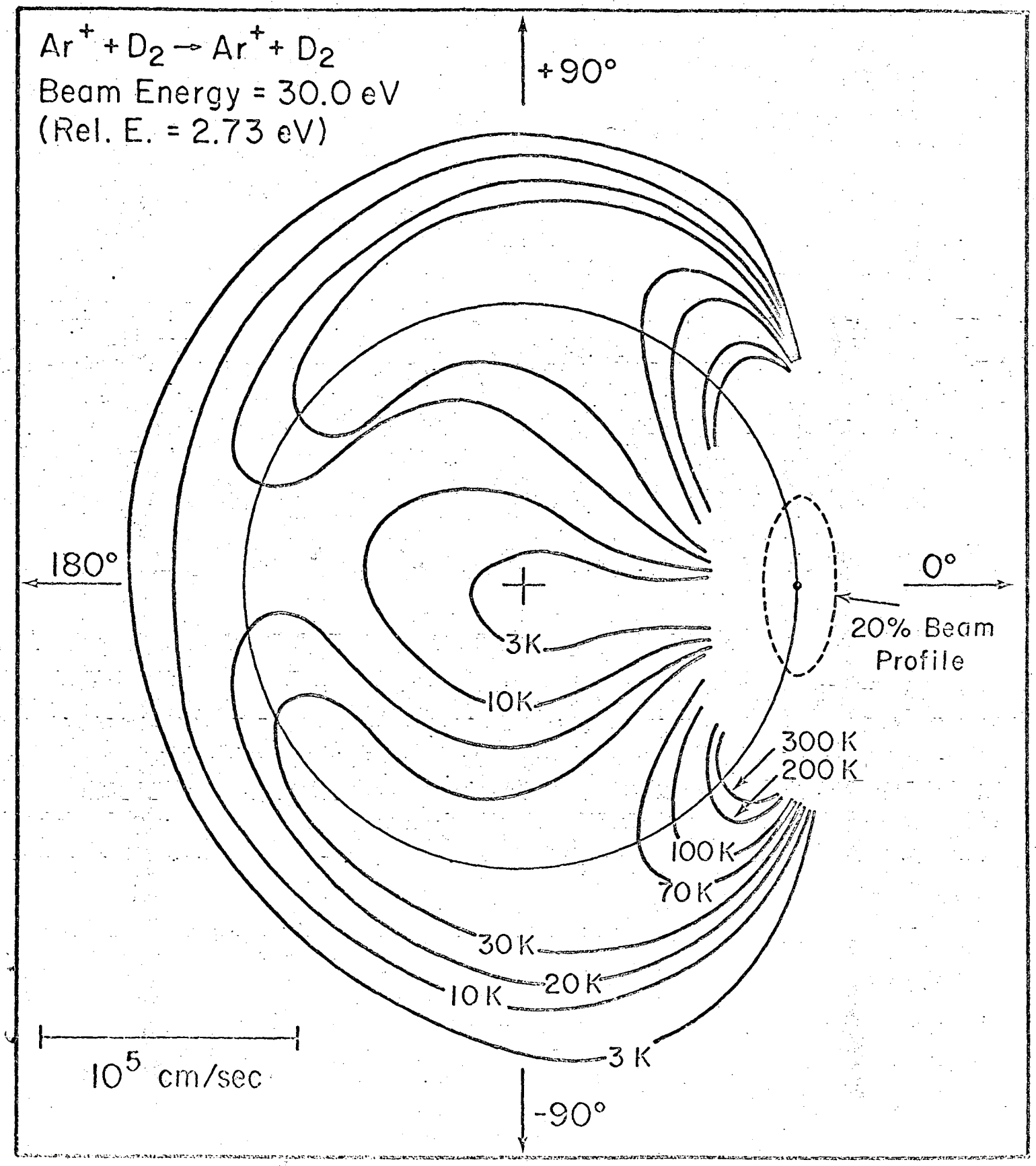
$Ar^+ + D_2 \rightarrow Ar^+ + D_2$
Beam Energy = 30.0 eV
(Rel. E. = 2.73 eV)
+90°
180°
0°
-90°
20% Beam Profile
3K
10K
300 K
200 K
100 K
70 K
30 K
20 K
10 K
3 K
10^5 cm/sec

Fig. 2

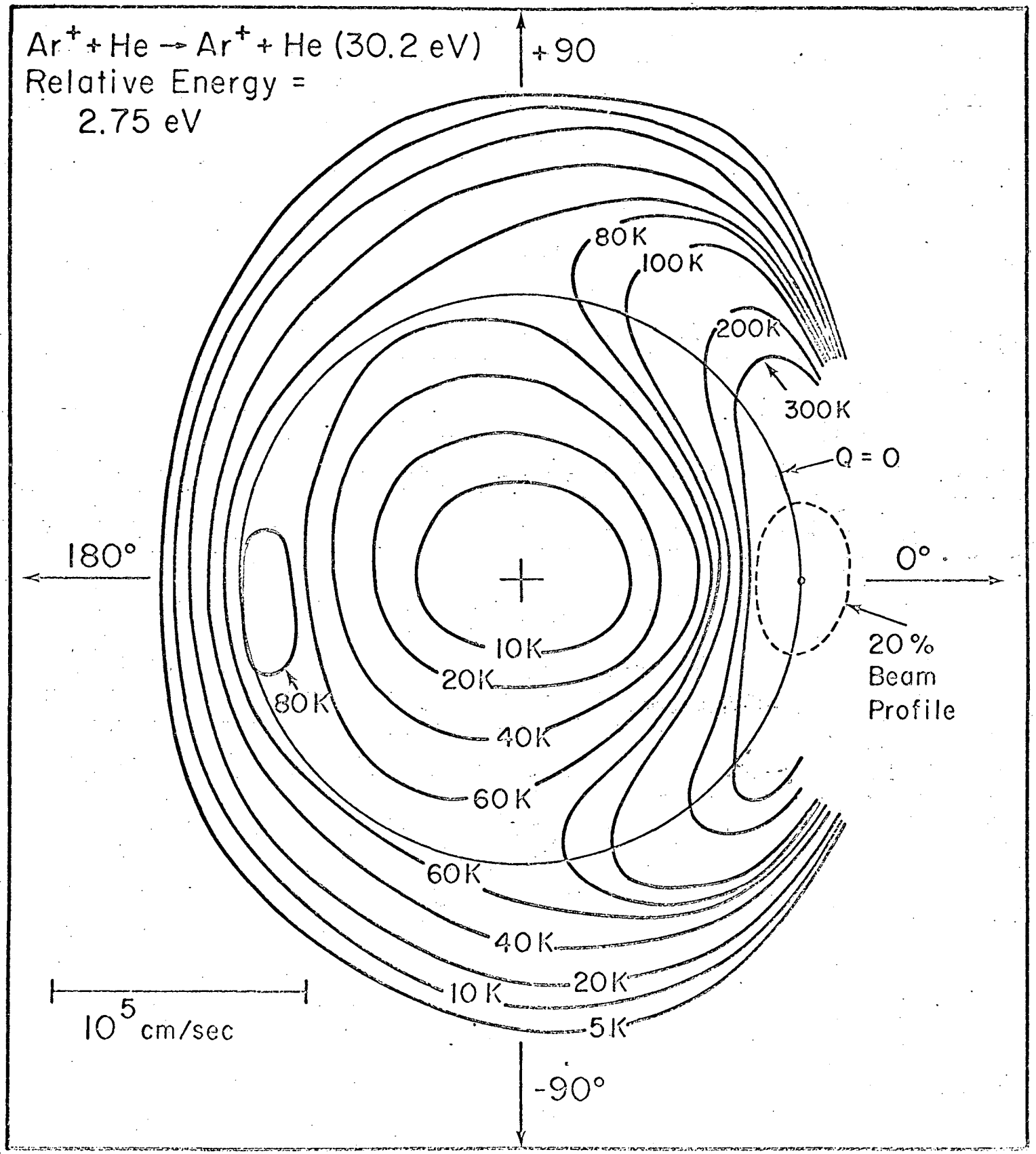
Ar+ + He → Ar+ + He (30.2 eV)
Relative Energy =
2.75 eV
+90
80K
100K
200K
300K
Q = 0
180°
0°
10K
20K
40K
60K
80K
20 %
Beam
Profile
60K
40K
20K
10K
5K
10^5 cm/sec
-90°

Fig. 3

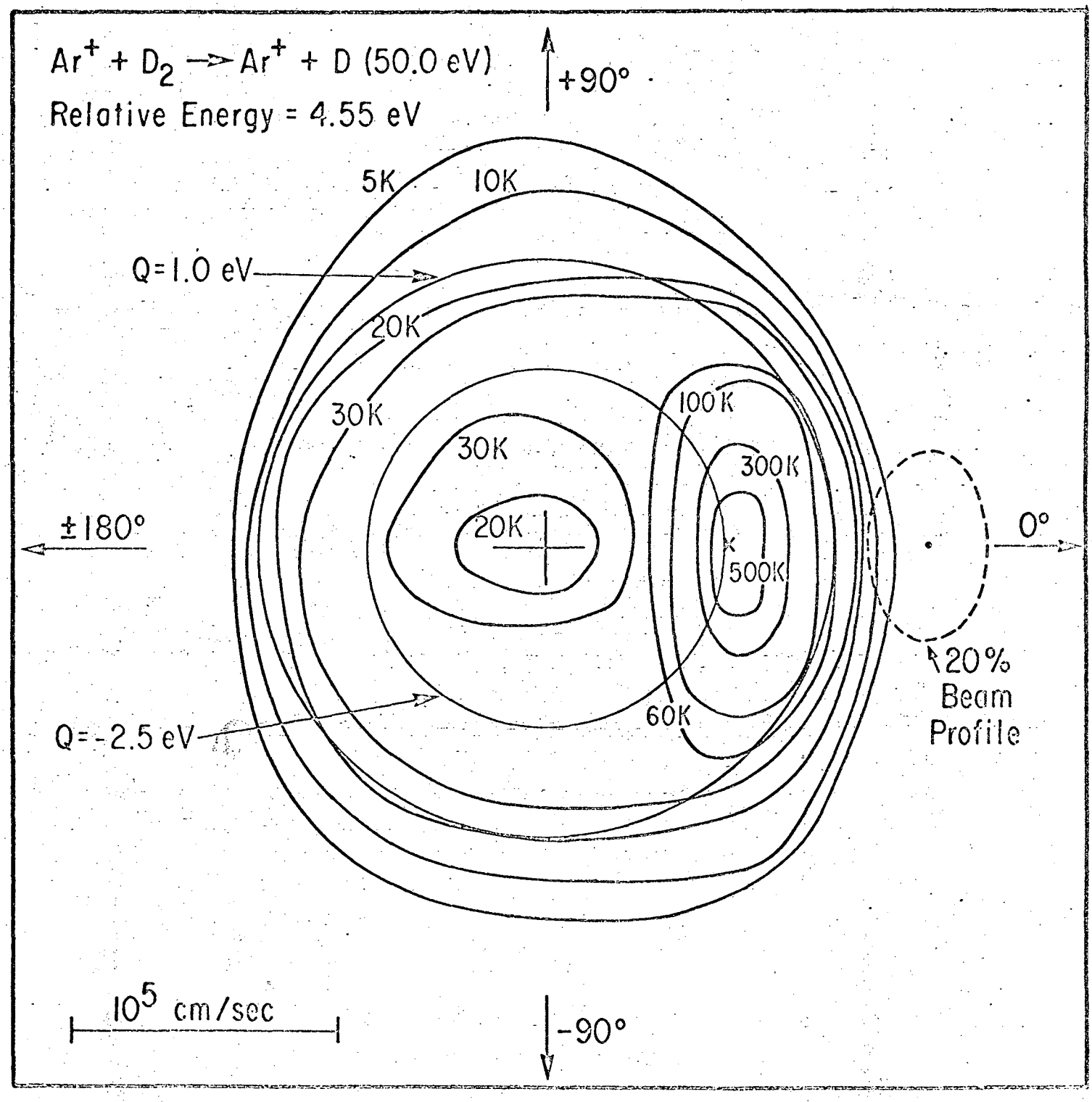
$Ar^+ + D_2 \rightarrow Ar^+ + D$ (50.0 eV)
Relative Energy = 4.55 eV
+90°
5K
10K
Q=1.0 eV
20K
30K
100K
30K
300K
±180°
20K
0°
500K
20% Beam Profile
60K
Q=-2.5 eV
10^5 cm/sec
-90°

Fig. 4

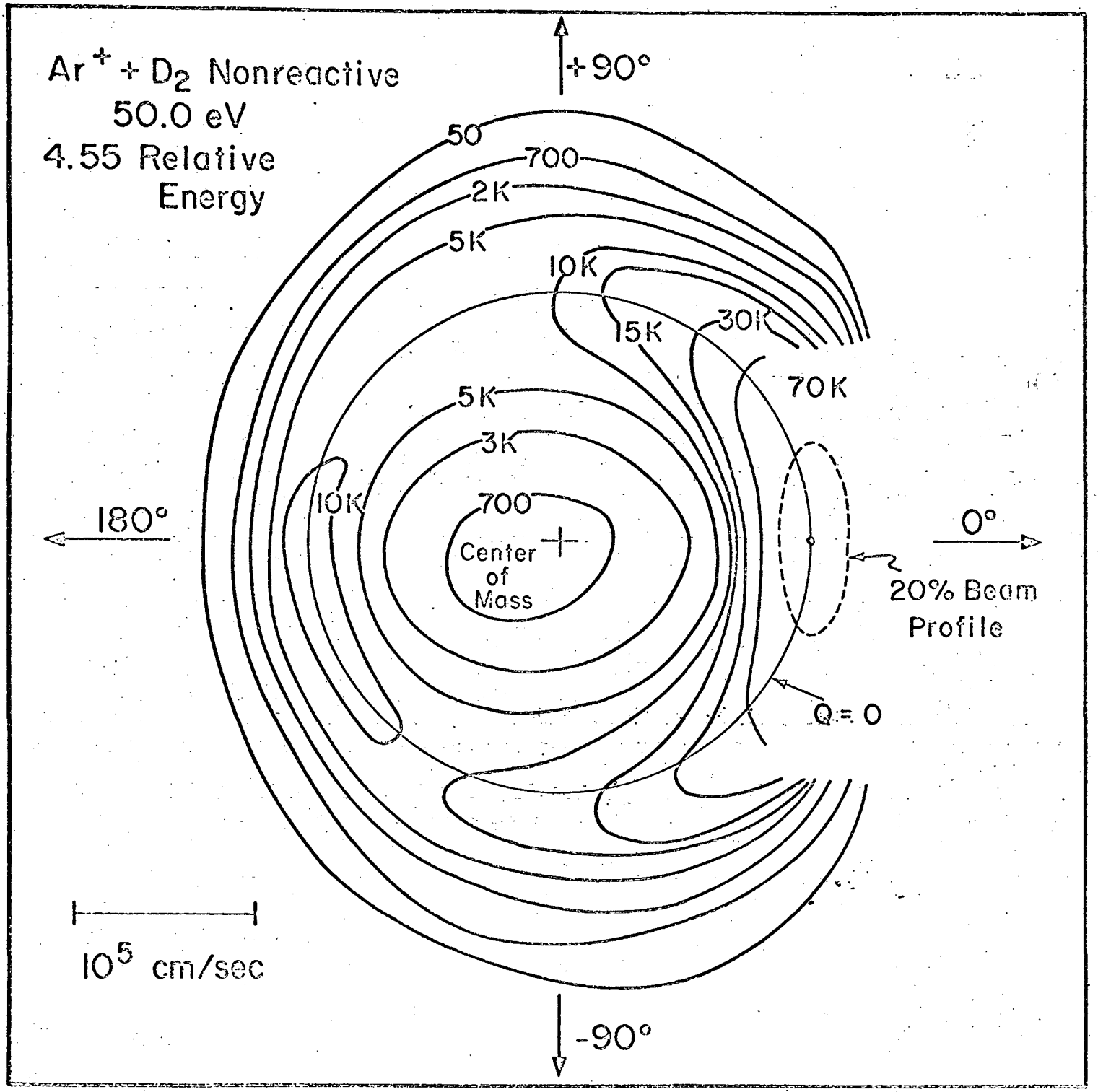
Ar+ + D2 Nonreactive
50.0 eV
4.55 Relative Energy
+90°
50
700
2K
5K
10K
15K
30K
70K
5K
3K
10K
700
Center of Mass
180°
0°
20% Beam Profile
Q = 0
10^5 cm/sec
-90°

Fig. 5

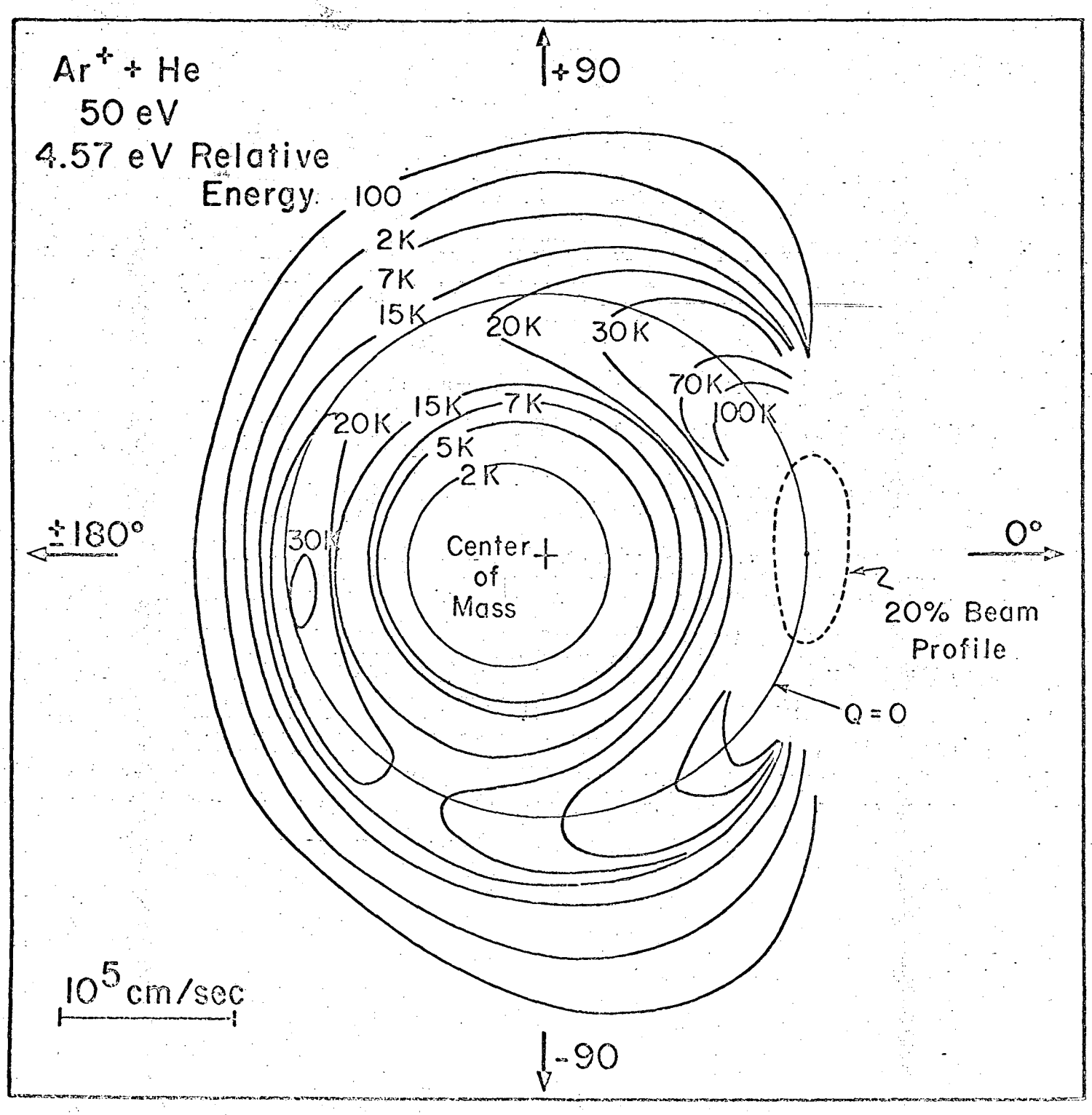
Ar+ + He
50 eV
4.57 eV Relative Energy
+90
±180°
0°
-90
100
2K
7K
15K
20K
30K
70K
100K
20K
15K
7K
5K
2K
30K
Center of Mass
20% Beam Profile
Q = 0
10^5 cm/sec

Fig. 6

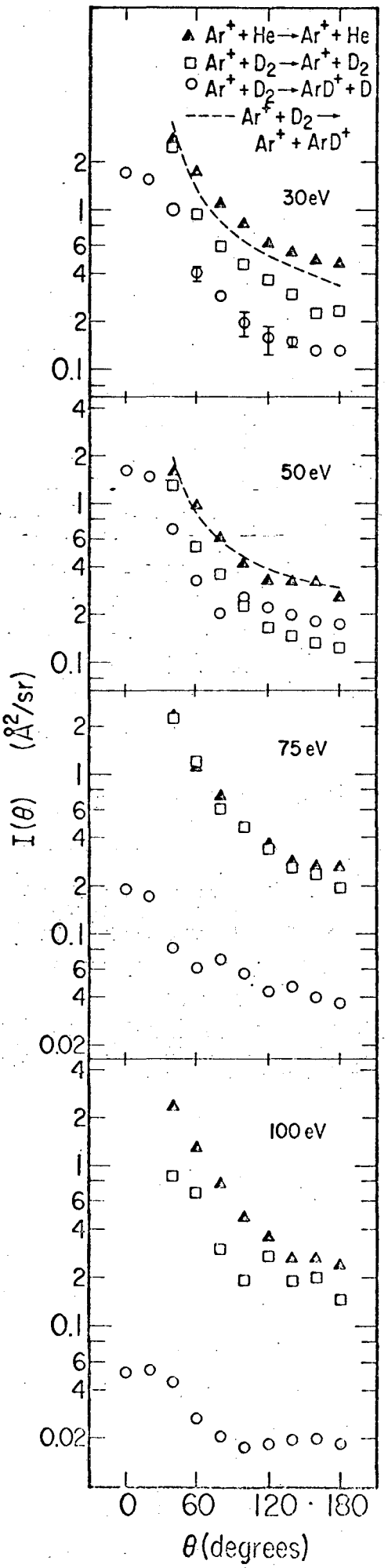
▲ $Ar^+ + He \rightarrow Ar^+ + He$
□ $Ar^+ + D_2 \rightarrow Ar^+ + D_2$
○ $Ar^+ + D_2 \rightarrow ArD^+ + D$
---- $Ar^+ + D_2 \rightarrow Ar^+ + ArD^+$
30eV
50eV
75eV
100eV
$I(\theta)$ $(Å^2/sr)$
θ(degrees)
0
60
120
180

Fig. 7

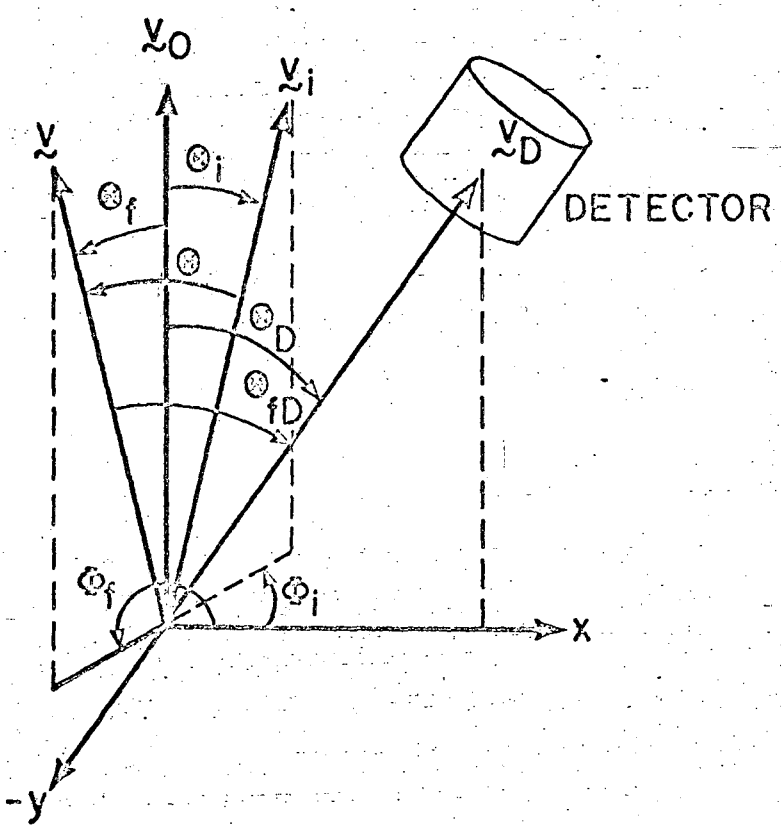
$\underset{\sim}{v}_o$
$\underset{\sim}{v}_i$
$\underset{\sim}{v}$
$\underset{\sim}{v}_D$
DETECTOR
Θ_i
Θ_f
Θ
Θ_D
Θ_{fD}
Φ_f
Φ_i
X
-y

Fig. 8

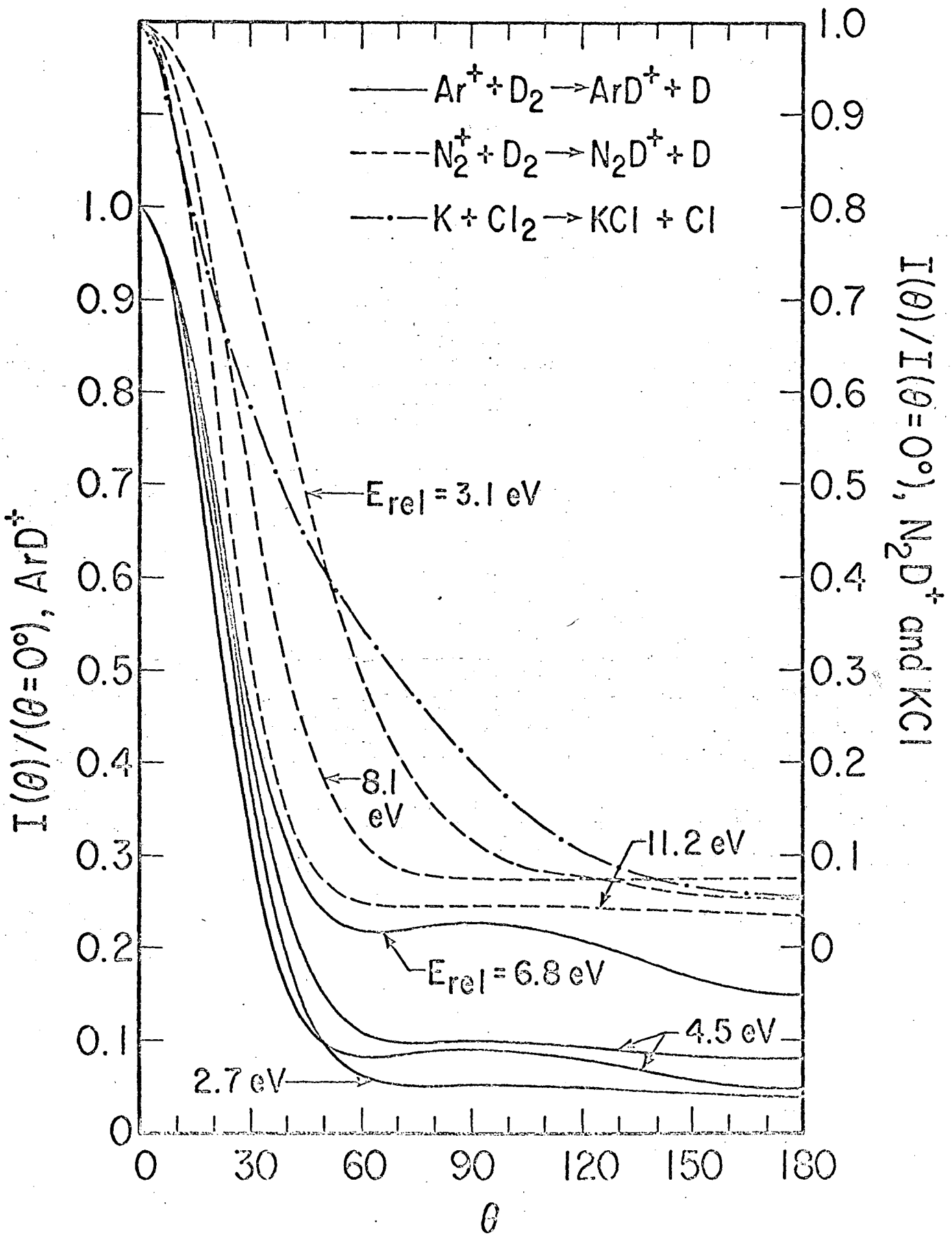
$Ar^+ + D_2 \rightarrow ArD^+ + D$
$N_2^+ + D_2 \rightarrow N_2D^+ + D$
$K + Cl_2 \rightarrow KCl + Cl$
$E_{rel} = 3.1$ eV
8.1 eV
11.2 eV
$E_{rel} = 6.8$ eV
4.5 eV
2.7 eV
$I(\theta)/(\theta=0°)$, ArD^+
$I(\theta)/I(\theta=0°)$, N_2D^+ and KCl
θ
0
30
60
90
120
150
180
0.1
0.2
0.3
0.4
0.5
0.6
0.7
0.8
0.9
1.0

Fig. 9

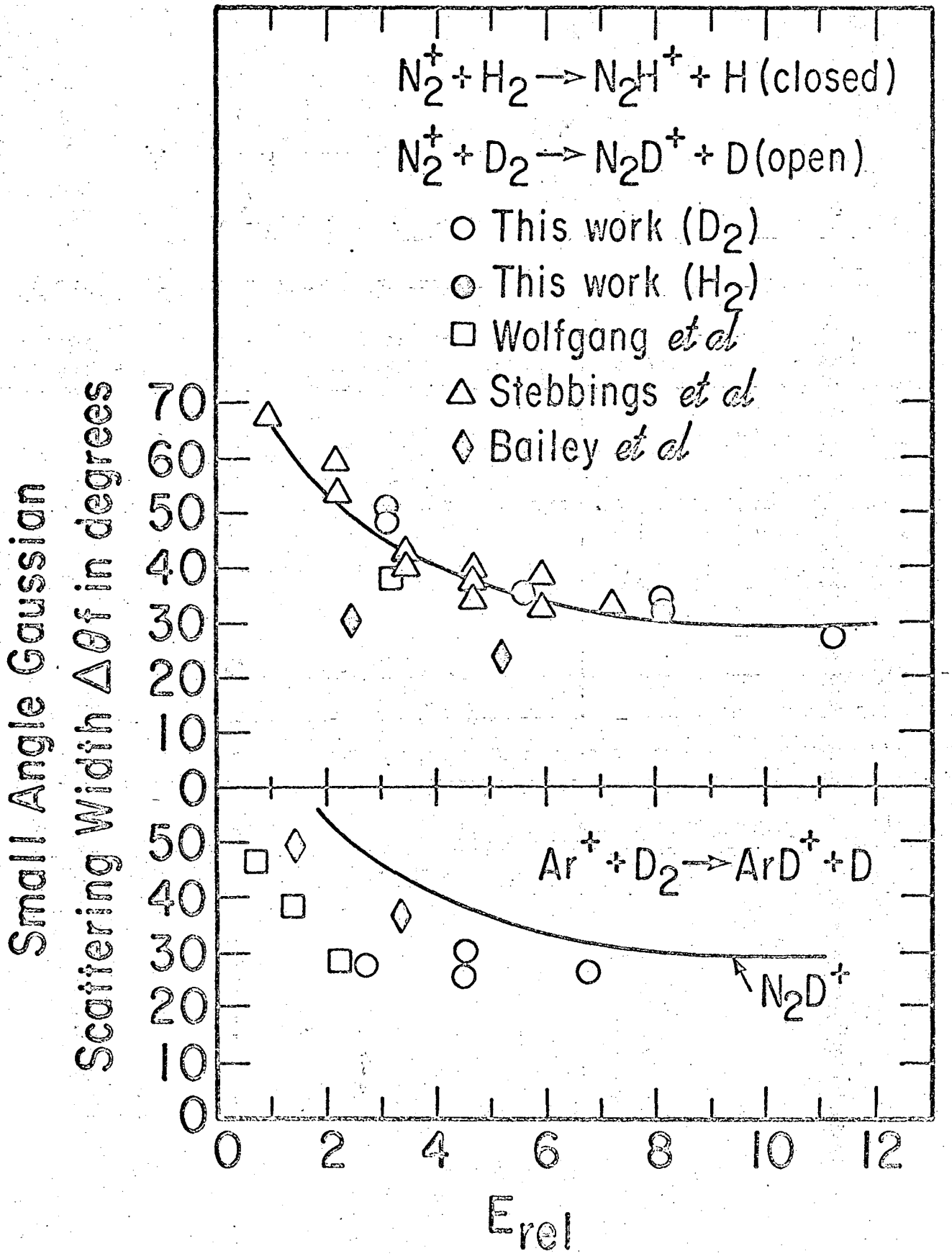
$N_2^+ + H_2 \rightarrow N_2H^+ + H$ (closed)
$N_2^+ + D_2 \rightarrow N_2D^+ + D$ (open)
This work (D_2)
This work (H_2)
Wolfgang *et al*
Stebbings *et al*
Bailey *et al*
$Ar^+ + D_2 \rightarrow ArD^+ + D$
N_2D^+
Small Angle Gaussian Scattering Width $\Delta\theta$ in degrees
70
60
50
40
30
20
10
0
50
40
30
20
10
0
0
2
4
6
8
10
12
E_{rel}

Fig. 10